PROCEEDINGS A

royalsocietypublishing.org/journal/rspa

Research

Cite this article: Shen J, Pirrera A, Groh RMJ. 2022 Building blocks that govern spontaneous and programmed pattern formation in pre-compressed bilayers. *Proc. R. Soc. A* **478**: 20220173.
https://doi.org/10.1098/rspa.2022.0173

Received: 13 March 2022
Accepted: 22 August 2022

Subject Areas:
mechanical engineering, computational mechanics

Keywords:
soft matter, bilayer wrinkling, bifurcations, pattern formation, spatial chaos, modal nudging

Author for correspondence:
Jiajia Shen
e-mail: j.shen@bristol.ac.uk

Electronic supplementary material is available online at https://doi.org/10.6084/m9.figshare.c.6179425.

THE ROYAL SOCIETY PUBLISHING

Building blocks that govern spontaneous and programmed pattern formation in pre-compressed bilayers

Jiajia Shen, Alberto Pirrera and Rainer M. J. Groh

Bristol Composites Institute (BCI), Department of Aerospace Engineering, University of Bristol, Bristol BS8 1TR, UK

JS, 0000-0003-2763-1147; AP, 0000-0003-3867-3916; RMJG, 0000-0001-5031-7493

Surface wrinkling in stiff-film/soft-substrate bilayers is a common phenomenon in biological systems and is increasingly being exploited in thin-film technology. While the onset of surface wrinkling in end-compressed bilayers is well understood, questions remain with regards to the evolution of the wrinkling pattern in the intermediate and deep post-wrinkling regimes, especially when the substrate is strongly pre-compressed. Here, we explore the bifurcation landscape of end-compressed bilayers with strongly pre-compressed substrates, using hyperelastic, plane strain finite-elements and generalized path-following algorithms. After bifurcating from a flat into a sinusoidally wrinkled state, bilayers undergo further n-tupling bifurcations into stable wrinkling patterns of longer wavelength whose periodicity $n = \{4, \ldots, 8\}$ is a function of overall bilayer length. These five n-tupling wrinkling patterns are shown to be independent localizations of the deformation mode and are accordingly identified as stable 'building blocks' that govern the intermediate post-wrinkling regime. Additional end-shortening into the deep post-wrinkling regime then leads to further period doubling and coalescence of the building blocks. Beyond a certain length threshold, a bilayer can form a combinatorial side-by-side arrangement of the five building blocks. In the limit of an infinitely long bilayer, this leads to the phenomenon known as spatial chaos with the emergence of an infinite

set of possible wrinkling patterns. In reality, though, the precise side-by-side arrangement of the building blocks is governed by the initial conditions. We show that the morphological evolution of the wrinkling pattern can be programmed by a judicial placement of manufactured dents in the thin film, creating new manufacturing capabilities for textured bilayers.

1. Introduction

Owing to their intrinsically low elastic modulus, soft materials and structures are highly susceptible to instabilities in response to internally or externally applied stimuli [1]. Instabilities in the form of wrinkling, folding and creasing can be critical for function in biological systems [2–5]. Malformation of such instabilities may lead to abnormal evolution of tissues or organs, which is often related to disease. Simultaneously, instability-induced morphologies are being used in advanced technologies, such as photovoltaic devices [6], flexible electronics [7], metrology methods [8] and microlens arrays [9]. Therefore, an understanding of morphological instabilities in soft materials not only facilitates the characterization of morphogenesis in biological systems, but also serves as a basis for the design of novel soft engineering systems [10]. In this paper, we focus on the nonlinear wrinkling behaviour of initially flat, stiff-film/soft-substrate bilayer systems with a pre-compressed substrate. Particular attention is given to the advanced post-wrinkling regime.

(a) Wrinkling onset

Extensive research has been conducted on the onset of wrinkling in end-compressed bilayers with different pre-strain levels applied to the substrate [11–14]. Closed-form equations have been derived to determine the compressive strain for which the bilayer transitions from an initially flat state to a periodic sinusoidal one (primary wrinkling/critical state), for cases where the stiffness ratio between the stiff film and the soft substrate is large [15,16]. The accuracy of these analytical solutions has been verified using finite-element (FE) methods [17]. The analytical solutions have also been used to back-calculate the material constants of bilayers in experimental tests [18] and for precision measurements [8].

(b) Post-wrinkling regime

With further compression beyond the primary critical state, the sinusoidal wrinkling mode loses stability at further bifurcations. Pre-strain in the substrate changes a bilayer's bifurcation diagram beyond the first (critical) bifurcation point in a significant way, particularly when the pre-strain level is high [18,19].

(i) No substrate pre-strain

For the case where the substrate is not pre-strained, the sinusoidal wrinkling pattern doubles in period at secondary supercritical bifurcations [16,20–24]. These sequential period doubling bifurcations as shown in figure 1*a*—i.e. period doubling followed by periodic quadrupling, etc.—have also been comprehensively described and reproduced using analytical [21,25] and FE methods [15,26–28].

Note that in all equilibrium manifolds shown we adopt the reaction force at the top right corner as the vertical axis instead of the widely used wrinkling mode amplitude. The reaction force correlates with the formation of a valley or a ridge in the wrinkling pattern. Specifically, when a valley forms and deepens, the reaction force increases, and when a valley becomes shallower, the reaction force reduces. Alternative measures, such as the amplitude of the wrinkling pattern, were considered less intuitive for depicting the pattern formation. For example, in the case

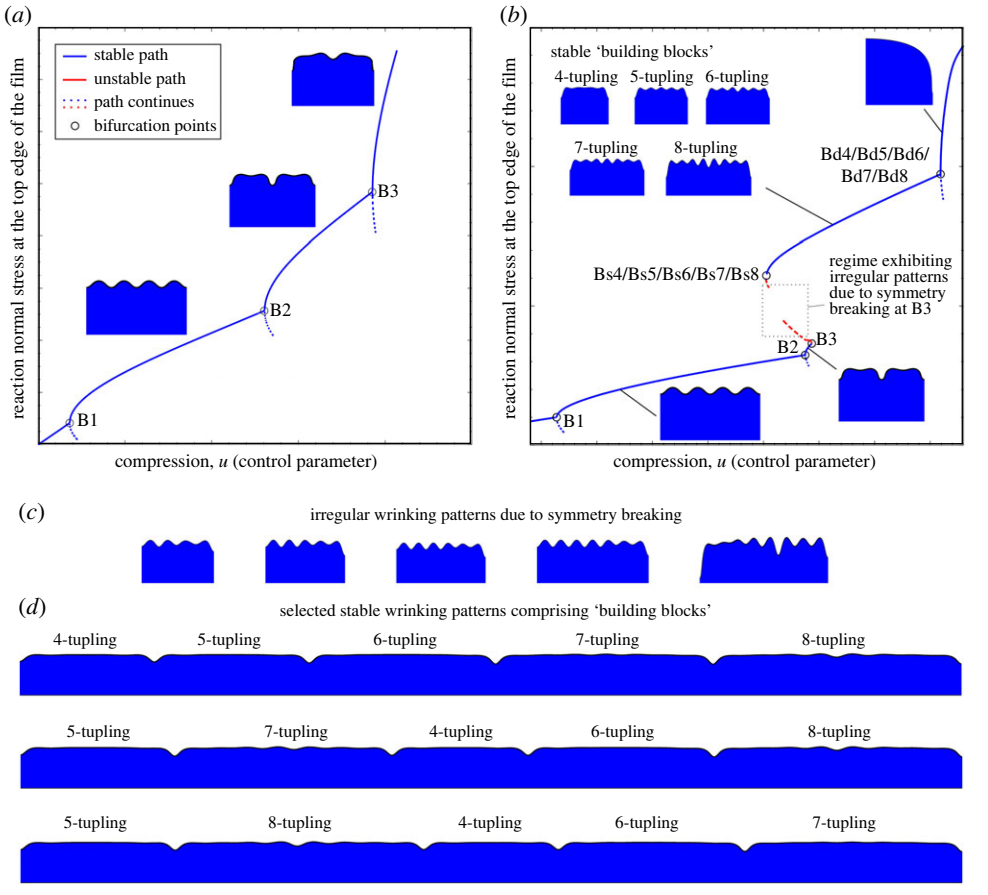

Figure 1. Schematic equilibrium diagram (reaction normal stress at the right corner of the top edge of the film versus compression u) of bilayers under end-compression with (*a*) unstrained substrate and (*b*) pre-compressed substrate. For bilayers with unstrained substrate, the post-wrinkling regime is governed by sequential supercritical bifurcations that double the wrinkling period. For bilayers with pre-compressed substrate, the equilibrium path destabilizes shortly after the first period doubling bifurcation, leading to irregular symmetry-breaking patterns shown in (*c*). Depending on bilayer length, restoration of stability leads to different period n-tupling modes $n = \{4, \ldots, 8\}$, which are here defined as stable 'building blocks'. The end-compression region over which the building blocks are stable is defined as the intermediate post-wrinkling regime. Additional compression beyond this leads to further period doubling, and for longer bilayers, coalescence of smaller building blocks (defined as the deep post-wrinkling regime). (*c*) Irregular wrinkling patterns due to symmetry breaking at B3 in (*b*). The irregular patterns correspond to period n-tupling mode $n = \{4, \ldots, 8\}$. (*d*) Selected stable wrinkling patterns in the intermediate post-wrinkling regime of a very long bilayer. The long bilayer can break into different combinations of the n-tupling building blocks identified in (*b*). The arrangement of different building blocks of varying length is strongly affected by initial imperfections, which explains the seemingly 'chaotic' wrinkling patterns observed in experiments. (Online version in colour.)

of subcritical bifurcations that lead to mode interaction and non-symmetric, irregular-looking wrinkling patterns, a single wrinkling amplitude is not informative in quantifying the wrinkling pattern.

(ii) Substrate pre-tensioning

Pre-tension in the substrate biases the stiff film to deflect outwards, leading to the formation of localized ridges [13,19,29]. Pre-tension also delays the onset of secondary bifurcations, i.e.

the sinusoidal wrinkling mode remains stable over a larger region of applied compressive strain [18,30]. Indeed, if the pre-tension strain is sufficiently pronounced, the sinusoidal wrinkling pattern eventually transitions to localized ridges directly, without the formation of period doubling bifurcations [13,31]. By adopting an FE model of length 9× the critical wrinkling wavelength with symmetric boundary conditions applied at both ends, Jin *et al.* [13] reproduced the transition of sinusoidal wrinkling to localized ridges that were observed in experiments.

(iii) Substrate pre-compression

A pre-compressed substrate biases the stiff film to deflect inwards, leading to the formation of folds [18]; see figure 1*b*. Moreover, pre-compression leads to a closer spacing of higher-order bifurcations on the *fundamental equilibrium path* (the locus of flat, purely compressed, solutions), resulting in mode interaction, imperfection sensitivity and patterns with a variety of interacting periodicities. As a result of the difficulty in predicting the evolution of wrinkling patterns into the deep post-wrinkling regime, and of the observed pronounced sensitivity to initial conditions, the literature describes the pattern formation of pre-compressed bilayers as 'chaotic' [18], independently of their length.

The origin of this seemingly 'chaotic' wrinkling response is difficult to pinpoint experimentally or using the nonlinear implicit solvers embedded in commercial FE packages. This is because, in order to trace post-wrinkling equilibrium paths with standard implicit/explicit FE solvers, possible bifurcation points need to be known *a priori* and either specific geometric imperfections, specific boundary conditions, or specific system lengths enforced to trigger the desired wrinkling mode. An improper choice of the perturbation profile or amplitude can lead to unrealistic wrinkling modes [32]. Therefore, an analysis based solely on standard FE solvers cannot provide the complete wrinkling landscape of pre-compressed bilayer systems.

Although a complete exploration of a bilayer's post-wrinkling stability landscape under substrate pre-compression is difficult, research has been conducted to understand the mechanics underlying their equilibrium manifolds, bifurcations and 'chaotic' pattern formation. Auguste *et al*. [18] adopted FE models with specific cell sizes, boundary conditions and geometric perturbations to accommodate certain wrinkling modes. The strain energy density corresponding to each wrinkling mode was computed and the wrinkling mode with the lowest energy then treated as the most favourable. Computational results revealed that the strain energies of period tripling and period quadrupling modes are comparable in the post-wrinkling regime, and this was suggested as a possible explanation for the coexistence of these two wrinkling modes in experiments. Xu *et al*. developed latticed models [33] and an asymptotic modelling and resolution framework [34] to trace the post-wrinkling behaviour of bilayers with pre-strained substrate. A period-tripling mode is observed when the substrate is highly pre-compressed. Note that the depth ratio between the film and substrate in these numerical models is less than 60. However, it is unclear if this ratio is sufficient to satisfy the infinite-depth assumption of the substrate. In the authors' experience, period tripling is a possible stable wrinkling pattern for shallower substrates, but vanishes as the substrate depth is increased (see the electronic supplementary material). Liu & Bertoldi [17] developed a numerical approach based on Bloch wave analysis to detect successive bifurcations on the equilibrium path of an infinitely long, end-compressed bilayer. Compared with standard nonlinear FE simulations performed on finite-size models, the method only requires a single unit cell, making the approach computationally efficient. With this method, Liu and Bertoldi found that the strains of the first few critical modes are very closely spaced and period quadrupling and period quintupling modes could form when the substrate is sufficiently pre-compressed. However, the convergence of the method is reported to be slow and the approach is invalid when the periodicity in the wrinkling mode is lost. To trace irregular wrinkling responses beyond certain bifurcations, path-following methods applied to systems longer than a single unit cell are therefore required.

(c) Research aims and outcomes

The analysis limitations highlighted in §1b(iii) above lead to the conclusion that robust path-following techniques that can detect critical points and automatically branch-switch onto secondary paths without recourse to initial imperfections are needed to explore the stability landscape of wrinkling bilayers with pre-compressed substrates and of generic length. Therefore, the objective of the research presented in this paper is to perform such explorations using the generalized path-following solver developed in [35,36], coupled with a hyperelastic, plane strain FE model. By performing said explorations, we uncover new phenomena and meet our aim of justifying currently unexplained experimental results on the end-compression of stiff-film/soft-substrate bilayers with pre-compressed substrates. That is

- Beyond the initial sinusoidal wrinkling regime, bilayers undergo n-tupling bifurcations into stable wrinkling patterns of longer period, with the periodicity n being a function of the overall bilayer length; see figure 1*b*. Five different n-tupling patterns are possible ($n = \{4, \ldots, 8\}$), which are here denoted as stable 'building blocks' of the intermediate post-wrinkling regime.
- While period doubling and period-quadrupling bifurcations in bilayers with an unstrained substrate are stable supercritical events, a pre-compressed substrate leads to subcriticality and irregularity, i.e. non-periodic patterns with broken left-right symmetry; as indicated in figure 1*c*. These irregular patterns represent intermediate transition modes that eventually, for increasing end-compression, connect to regular periodic solutions. Furthermore, for some levels of compression, the irregular patterns coexist with the periodic solutions. In other words, the system may display multistability, thereby explaining the seemingly 'chaotic', but actually just irregular and multivalued, response of the wrinkle formations observed in previous experiments [18].
- Beyond a threshold length, a long bilayer bifurcates into a specific side-by-side arrangement of the five stable building blocks. Of all possible permutations of building blocks that can tessellate the bilayer's extension, the sequence observed experimentally is defined by the initial conditions. Hence, the morphological evolution of the wrinkling pattern is deterministic but exceedingly imperfection sensitive as the bilayer length increases. Long, perfect bilayers can then actually be said to behave in a spatially chaotic manner [37].
- As a corollary, the evolution of the wrinkling pattern for increasing end-compression can be programmed by controlling the initial conditions, e.g. through small localized dents in the thin film.

The remainder of the paper is structured as follows. Section 2 provides a brief background of the FE formulation for the two-dimensional plane strain elements for compressible hyperelastic materials, considering pre-strain effects. In §3, we present the effects of bilayer length on the wrinkling landscape. Further insights are shed in §4. Section 5 presents a method to tailor the post-wrinkling behaviour of bilayers using localized dents. Finally, conclusions are drawn in §6.

2. Methods

(a) Finite-element formulation and generalized path-following technique

An in-house nonlinear FE program [36] is used to investigate the response of bilayers comprised of a stiff, thin-film mounted on a soft, pre-compressed substrate. A plane strain condition in the width direction of the bilayers is assumed and therefore planar finite-elements used to discretize the length and transverse dimensions (figure 2). Both film and substrate are modelled using

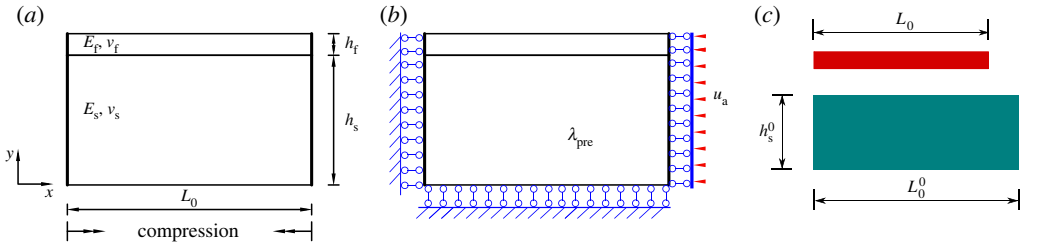

Figure 2. (*a*) Geometry and loading condition of the film/substrate bilayer system. (*b*) Boundary conditions of the bilayer system in the FE model. (*c*) The geometry of the compliant substrate and stiff film before pre-compression of the substrate. (Online version in colour.)

a compressible Neo-Hookean hyperelastic material model [38]. A 'nearly' incompressible Neo-Hookean material (with incompressibility enforced using a penalty constraint [38]) was also implemented, with minor quantitative and no qualitative changes to the bifurcation manifolds. The Neo-Hookean material features parameters that are recognized from a familiar linear elastic material model. The Helmholtz free energy of the compressible Neo-Hookean material is given by

$$\Phi = \frac{\mu}{2}(I_C - 3) - \mu \ln J + \frac{\lambda}{2}(\ln J)^2, \tag{2.1}$$

where $I_C = \mathrm{tr}\, \boldsymbol{C}$ and $J^2 = \det \boldsymbol{C}$, with $\boldsymbol{C} = \boldsymbol{F}^\top \boldsymbol{F}$ being the right Cauchy–Green deformation tensor derived from the deformation gradient tensor $\boldsymbol{F}$. Lamé's first parameter is given by $\lambda = E\nu/[(1+\nu)(1-2\nu)]$ and the shear modulus is expressed as $\mu = E/[2(1+\nu)]$, with E and ν representing Young's modulus and Poisson's ratio, respectively.

Pre-strain in the substrate is modelled using a multiplicative decomposition of the deformation gradient tensor $\boldsymbol{F} = \boldsymbol{F}_e \boldsymbol{F}_\Theta$. This decomposition represents a stress-free expansion/contraction of the substrate into an intermediate state (e.g. through growth, swelling or thermal expansion) via $\boldsymbol{F}_\Theta$, followed by an additional elastic and stress-inducing deformation via $\boldsymbol{F}_e$ that ensures compatibility with the attached film. In this paper, a thermal representation of the multiplicative decomposition is chosen for convenience, i.e. $\boldsymbol{F}_\Theta$ represents free thermal expansion of the substrate. The detailed theoretical derivation and the verification of the finite-element formulation can be found in §1 of the electronic supplementary material.

Apart from standard arc-length continuation methods, the in-house FE implementation features additional functionality for pinpointing limit and branching points directly, branch-switching at bifurcation points, and tracing critical points through parameter space. For completeness, a relatively concise but self-contained outline of the generalized path-following technique is also presented in §1 of the electronic supplementary material. A detailed exposition can be found in references [35,36]. With this nonlinear solver, we can explore the bifurcation landscape of the bilayer in a robust way without pre-existing knowledge of branching events. More importantly, we can trace certain critical and non-critical equilibria in parameter space, e.g. bilayer length and depth, directly, rather than conducting expensive parametric studies.

(b) FE model set-up

In this study, we consider bilayers as shown in figure 2*a*, discretized by 16-noded, isoparametric plane strain elements. The mesh is most dense towards the interface of the film/substrate and gradually coarsens towards the bottom of the substrate. The applied boundary conditions are shown in figure 2*b*. Horizontal displacement restraints are applied on the left end and horizontal compression is applied on the right end, leading to symmetry-enforcing boundary conditions at both ends. Vertical displacement restraints are applied on the bottom of the substrate. In order to satisfy the assumption that the substrate is infinitely thick and to guarantee that the influence

of the vertical restraint of the substrate's bottom edge on the system overall is negligibly small, the substrate depth needs to be as large as possible while balancing the associated computational cost.

Currently, there seems to be no consensus in the literature on the appropriate substrate depth to satisfy the infinite-substrate assumption. Specifically, Liu & Bertoldi [17] suggest a substrate depth 30 times the critical wrinkling wavelength—i.e. the wavelength, L_{crw}, at the transition from the flat to the sinusoidally wrinkled state—while Cao & Hutchinson [15] recommend $10L_{\mathrm{crw}}$. Conversely, Auguste *et al.* [18] suggest a substrate depth of 50 times the film thickness. Using the generalized path-following solver, a sensitivity study was conducted on the bilayer's response to varying substrate depth in the advanced post-wrinkling regime. Unsurprisingly, we found that the depth of the substrate required to satisfy the infinity assumption is dependent on the purpose of the analysis. If the deep post-wrinkling behaviour is of interest, a larger substrate depth is required compared with when only the critical wrinkling state or the initial post-wrinkling behaviour is of interest. A model with an insufficiently deep substrate not only gives inaccurate predictions of the post-wrinkling behaviour, but more importantly, leads to significant changes in the bifurcation structure. Therefore, alongside a classic mesh density study, a sensitivity study on the depth of the discretized bilayer is an essential pre-requisite for accurate FE analyses. Our analysis suggests that for the present model, and our goal of exploring the intermediate and deep post-wrinkling regimes, a substrate depth of 30 times the critical wrinkling wavelength is appropriate. The details of the depth sensitivity analysis can be found in §2 of the electronic supplementary material.

Pre-compression in the substrate is modelled by imposing free thermal expansion in the horizontal direction using orthotropic expansion coefficients, and then bonding the freely expanded substrate to the stiff film; see figure 2*c*. The mismatch in the free lengths of the film and the substrate places the substrate in compression before further mechanical end-shortening is applied. The details of the initial thermal loading step to pre-compress the substrate can be found in §1.3 of the electronic supplementary material. Further, the FE models were verified using existing numerical and experimental results from [18] and the mesh was refined until good convergence with these benchmark solutions was obtained. This verification of the FE model is also presented in §1.5 of the electronic supplementary material.

3. Effect of bilayer length on the post-wrinkling behaviour

Previous work has focused on the critical wrinkling formation of bilayers with a specific length and suitably applied symmetry conditions at the left and right extremities, where the total length of the system was taken to be an integer multiple of the critical wrinkling wavelength, L_{crw}. As is shown in this paper, geometric and material imperfections introduced during manufacturing can divide long bilayers with strongly pre-compressed substrates into several segments of defined lengths that deform independently. As compression is increased, these deformation patterns of finite length evolve and may coalesce, seeding the formation of humps separated by fold localizations. Owing to the latter considerations, a length sensitivity study is important to understand the mechanics of bilayers in the intermediate and deep post-wrinkling regimes.

Table 1 presents the geometry and material properties of the film/substrate bilayer system in this length sensitivity study. The parameters chosen are identical to those by Brau *et al.* [21]. The pre-compression level, λ_{pre}, in the substrate is set as 0.7, i.e. $\lambda_{\mathrm{pre}} = L_0/L_0^0 = 0.7$, where L_0 is the length of the bilayer after pre-compression and L_0^0 is the initial length of the substrate before pre-compression. These geometric parameters are depicted schematically in figure 2*c*. For the chosen level of pre-compression, seemingly 'chaotic' wrinkling patterns were observed experimentally [18].

To begin our analysis, a study of the critical wrinkling behaviour for varying bilayer length is conducted to determine the critical wrinkling wavelength, L_{crw}, and the critical wrinkling strain, $\varepsilon_{\mathrm{crw}}$. The details of this analysis are presented in §3 of the electronic supplementary material. For the bilayer with properties presented in table 1, $L_{\mathrm{crw}} = 5.34\,\mathrm{mm}$ and $\varepsilon_{\mathrm{cr}} = 0.0163$.

Table 1. Material and geometric properties of the stiff film/compliant substrate system.

E_f (MPa)	E_s (MPa)	ν_f	ν_s	h_f (mm)	h_s (mm)
1.2	0.01	0.43	0.43	0.2	160

More importantly, we then proceed to exploring the post-critical behaviour of bilayers of different lengths to unveil their bifurcation diagrams using the generalized path-following solver. These analyses explore the evolution of the wrinkling pattern from the critical sinusoidal mode into n-tupling patterns with pronounced downward localizations (folds) at one or both ends of the bilayer, which eventually lead to an upward hump forming in-between. As an important outcome, we show that there is a minimum and a maximum possible distance between two adjacent localizations, i.e. a minimum and a maximum possible length for the n-tupling modes that evolve into a hump. As such, any bilayer system longer than the upper bound ultimately splits into an array of smaller 'building blocks' that fall within the allowable range. Detailed bifurcation analyses on bilayers with lengths ranging from $3L_{crw}$ to $9L_{crw}$ were conducted, the details of which can be found in §4 of the electronic supplementary material. For the sake of concise illustration, here, we present the equilibrium path of a select three characteristic cases, i.e. $L_0 = 5L_{crw}$, $L_0 = 9L_{crw}$ and $L_0 = 4.445L_{crw}$, which exemplify the behaviour of bilayers with overall length within and outside the domain of existence of the identified building blocks, and of bilayers of length equal to a non-integer multiple of the critical wavelength. Note that the full wrinkling stability landscape of bilayers features a large number of equilibrium paths due to numerous successive bifurcations. For clarity and brevity, only those paths that lead to the final stable hump mode with fold localizations at either or both boundaries are presented here.

(a) $L_0 = 5L_{crw}$

Figure 3*a* presents the bifurcation diagram of a bilayer with length $L_0 = 5L_{crw}$, plotted in terms of engineering strain (Δ/L_0) versus the reaction force at the top right node of the film in the FE model, normalized by its value at the onset of wrinkling. The blue segment in the bottom left-hand corner is the stable equilibrium path corresponding to the initially flat state. As compression is increased, the flat state loses stability at a supercritical pitchfork bifurcation (point B1) and the bilayer transitions onto the critical sinusoidal wrinkling mode with five full waves; see figure 3*c*, which also features the rest of the salient deformation modes. The sinusoidal wrinkling mode is stable up to the secondary bifurcation point B2. The critical eigenmode at B2 corresponds to a period doubling bifurcation (figure 3*b*) that breaks left-right symmetry and leads to a wrinkling mode similar to those in bilayers with no pre-strain in the substrate [22]. However, beyond B2, the period doubling pattern quickly loses stability at a subsequent subcritical bifurcation denoted as B3. Branch-switching at B3 leads to an unstable equilibrium path and the formation of an inward localization at the right end of the bilayer, owing to the loss of periodicity and further disruption of the left-right symmetry group. Stability is then restored and lost again at limit points LP1 and LP2, respectively. Path-following further, the left-right symmetry is restored at the pitchfork bifurcation point B4, which connects to a period quintupling mode. A further period doubling sequence is triggered at bifurcation point B5, where period quintupling loses stability and the wrinkling mode's periodicity doubles again to become 10-fold. For the present model, no additional mode changes are observed beyond this point, with a crease (contact across a symmetry line) forming at the right end of the domain at the nominal compressive strain of $\Delta/L_0 = 0.1057$.

Let us now focus with renewed attention on the region of the bifurcation diagram of strain comprised between limit points LP1 and LP2. As mentioned above, the stable equilibria connecting the limit points have an irregular—meaning non-periodic—wrinkling pattern. Conversely, either side of this region the bilayer exhibits regular periodic deformation modes. To the left, we find a simple periodic mode; to the right, one with localized boundary folds. It

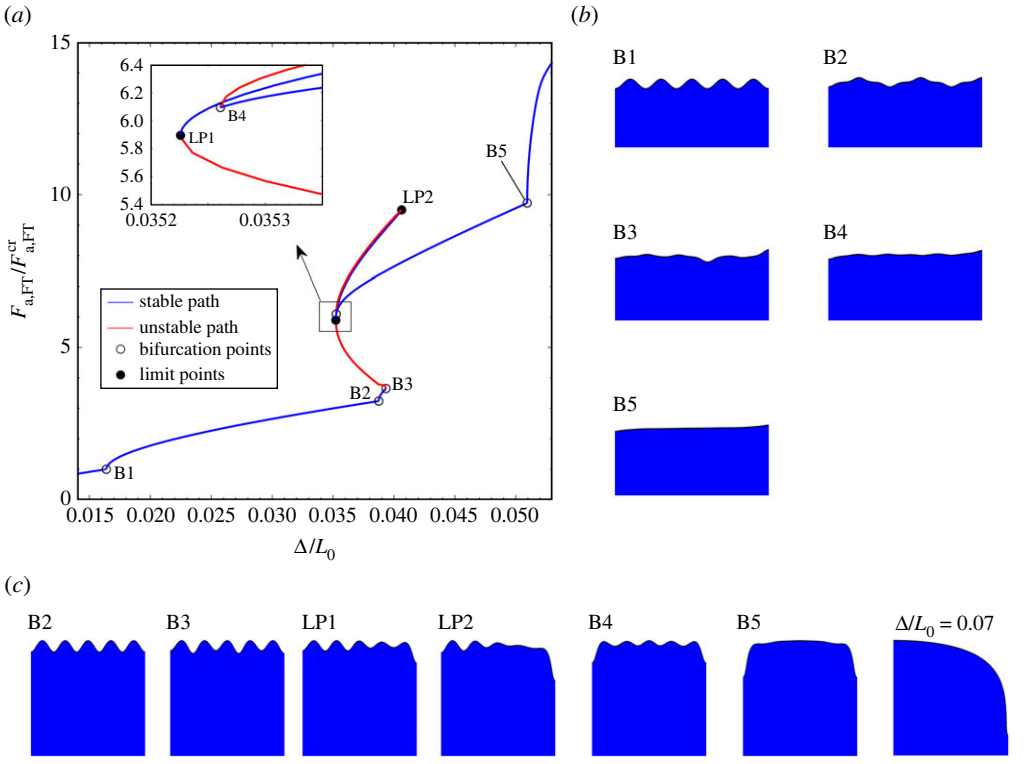

Figure 3. Equilibrium path and wrinkling modes of a bilayer with length $L_0 = 5L_{crw}$ and pre-compression strain in the substrate of 0.7. (*a*) The normalized reaction force at the top node of the film $F_{a,FT}/F^{cr}_{a,FT}$ versus compressive engineering strain Δ/L_0. $F^{cr}_{a,FT}$ is the force at the top node at the critical wrinkling point B1. (*b*) Critical eigenmodes at bifurcation points, and (*c*) the wrinkling modes at critical points. To aid visualization, the wrinkling modes have been amplified by a factor of 5. The depth of the substrate does not reflect the actual depth. Note that the full wrinkling stability landscape features significantly more equilibrium paths, and only those paths that lead to the final stable wrinkling mode with a localization at either or both boundaries are presented here. (Online version in colour.)

follows that the area with instabilities acts as a transition region separating two stable, periodic, yet qualitatively different responses to end shortening. It should also be noted that, for these values of end shortening, the system is multistable. The observed irregularity in the wrinkling pattern coupled with the multistability of the system may account for the seemingly 'chaotic' behaviour observed in experiments [18], while, in fact, our results reveal the deterministic nature of the bilayer's response, which, owing to the multistability, simply depends on imperfections and initial conditions.

Overall, the topology of the bifurcation diagram demonstrates the well-known tendency of bilayers to lengthen their wrinkling period sequentially under increasing applied compressive loads [21]. In contrast to bilayers without pre-compression, though—where the wrinkling patterns are always periodic with periods lengthening consistently in the same manner irrespective of the applied load, i.e. exclusively by sequential, supercritical, period doubling bifurcations—the pre-compressed bilayer initially loses said tendency but reacquires it past a certain level of compressive strain. In other words, the bilayer's behaviour can be described as having three post-wrinkling regimes: initial, intermediate and deep. To define the boundaries of these regimes, we need to look qualitatively at the different dynamic responses of the system for increasing end-compression.

The initial post-wrinkling regime is the region at low compressive loads where the bilayer behaves qualitatively like a bilayer with no pre-compression, i.e. the period of the deformation

mode lengthens by period doubling. Using this definition, in a quasi-static setting, the initial regime would be identified as extending from $\Delta/L_0 = 0$ to B3. However, in reality, the bilayer exhibits multistability, that is, intermediate-type behaviour with period lengthening caused by traversal of regions of instability and non-periodic modes, from LP1. So, in conclusion, considering the potential for dynamic shape transitions, the bilayer displays post-wrinkling behaviour of the initial type from $\Delta/L_0 = 0$ to LP1. In other words, the initial post-wrinkling regime ends even before the first period doubling bifurcation (B2) occurs.

The intermediate regime coincides with the portion of the bifurcation diagram where the period of the deformation mode stops and then resumes lengthening exclusively by period doubling. As explained above, this transition starts at LP1. From LP1 to LP2, the bilayer may traverse the equilibrium manifold dynamically by jumping between different stable wrinkling modes that are irregular and aperiodic. Eventually, with a snap onto the period quintupling deformation mode after multistability is lost at LP2, left-right symmetry is also restored. The advanced intermediate post-wrinkling regime for the bilayer with a pre-compressed substrate is therefore governed by the stable period quintupling mode that forms an outward hump bounded by two inward localizations at either end of the domain.

Once this stable period quintupling mode has formed fully (at B5), we enter the deep post-wrinkling regime. The wrinkling pattern is periodic and again the periodicity doubles in length at supercritical pitchfork bifurcations. The deformation pattern past B5 is delimited by one localization at the right end of the domain only (see $\Delta/L_0 = 0.07$ in figure 3*c*). This deformation mode is one half of a period-decupling wrinkling pattern. Hence, a system of twice the length ($L_0 = 10L_{\mathrm{crw}}$) may feature two adjacent period quintupling blocks merging into one larger period decupling block in the deep post-wrinkling regime.

In conclusion, upon complete maturation of the period quintupling mode at B5, the bilayer with pre-compressed substrate reflects the behaviour of the corresponding bilayer with an unstrained substrate again, as it is governed by exclusively supercritical bifurcations that double the wrinkling period. The differentiating factor between the two systems is therefore the intermediate post-wrinkling regime (between LP1 and B5), where for a pre-compressed substrate, the period doubling mode loses stability and symmetry, and finally restabilizes in a symmetric period quintupling mode. The identified period quintupling mode (B4–B5) is here denoted as the 'building block' that characterizes the bilayer's behaviour in the intermediate post-wrinkling regime. Similar building blocks, ranging from period quadrupling to period octupling, are identified by modelling additional bilayer lengths extending from $L_0 = 4L_{\mathrm{crw}}$ to $L_0 = 8L_{\mathrm{crw}}$ (see §4 of the electronic supplementary material). The general topology of the bifurcation manifold is preserved in all cases—i.e. destabilization of the first period doubling mode; breaking and restoring of periodicity and symmetry to form a period n-tupling mode; and further stable doubling. The generic sequence is summarized schematically in figure 1*b*, where all possible stable building blocks of the intermediate post-wrinkling regime are shown. The name 'building block' encapsulates the defining attributes of these deformation patterns. A 'building block' has finite length. In longer bilayers, different building blocks can emerge as distinct localizations—reminiscent of *wrinklons* [39], the localized transition zones of merging wrinkles that form the building blocks of two-dimensional wrinkling patterns in thin sheets—and interface to build the deformation pattern over the full length of the bilayer. For greater applied strains, adjacent building blocks may coalesce to form more extensive hump-type geometries.

Demonstrating the aforementioned behavioural attributes of building blocks in longer bilayers is what we turn to next by studying a bilayer of length $L_0 = 9L_{\mathrm{crw}}$.

(b) $L_0 = 9L_{\mathrm{crw}}$

Figure 4 presents the equilibrium path, as well as the wrinkling modes and critical eigenmodes at selected equilibria, for a bilayer with $L_0 = 9L_{\mathrm{crw}}$. With the comprehensive parameter sweep presented in §4 of the electronic supplementary material, we found that a bilayer of this length breaks with the generic bifurcation structure occurring for $L_0 = [4, \ldots, 8]L_{\mathrm{crw}}$ and described

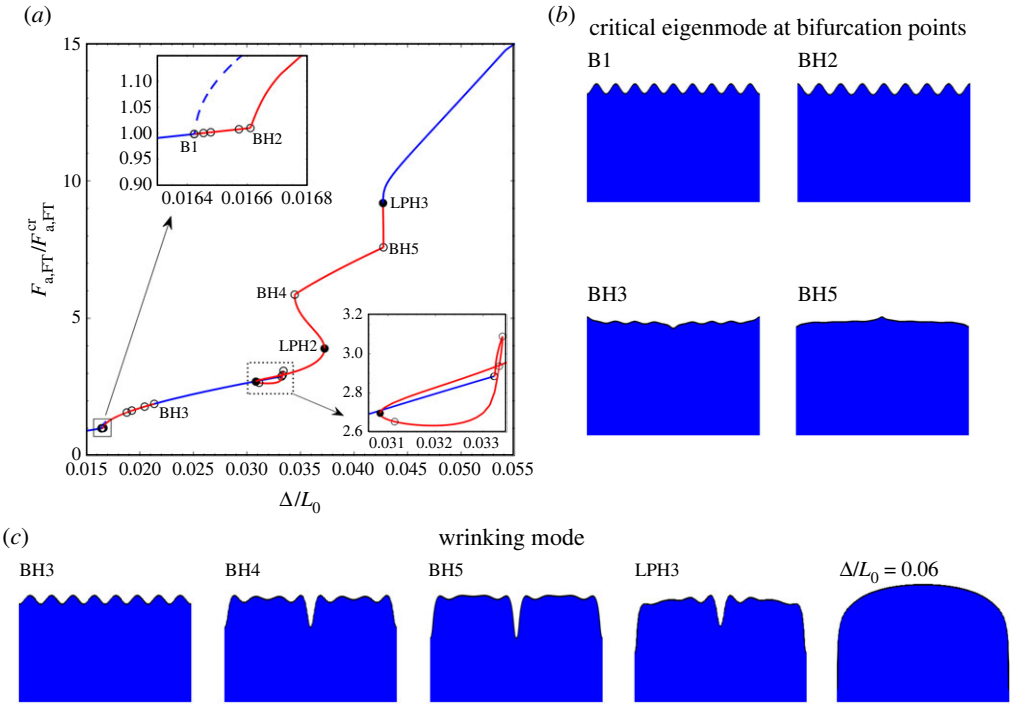

Figure 4. (*a–c*) Equilibrium path and wrinkling modes of a bilayer with length $L_0 = 9L_{crw}$ and pre-compression strain in the substrate of 0.7. Detailed annotations in the figure are as described in figure 3. The path leading to period nonupling bifurcates from BH2. The equilibria between B1 and BH2 are unstable. Hence, under natural loading (monotonically increasing end-shortening), the bilayer bifurcates at B1 and follows the stable primary path with nine sinusoidal wrinkling waves (see the dashed blue curves in the inset). Note that the bifurcation structure in the dashed rectangle is essentially the same as the case with $L_0 = 4.445L_{crw}$ in figure 5. (Online version in colour.)

in the previous section. That is to say, a bilayer of length $L_0 = 9L_{crw}$ does not form a stable period nonupling mode as a result of symmetry-breaking and -restoring in the intermediate post-wrinkling regime, but rather separates into shorter building blocks.

Indeed, figure 4 shows that a stable wrinkling mode forms in the intermediate post-wrinkling regime that is period octupling rather than period nonupling—intermediate-type behaviour occurring in this case between B1 and LPH3[1]—and it is this octupling mode that then leads to the formation of the full hump in the advanced post-wrinkling regime. In particular, as seen at points BH4 and BH5 of the equilibrium manifold, the period octupling deformation pattern separates into two period quadrupling modes (albeit unstable ones), which eventually coalesce into the stable period nonupling mode at LPH3. Hence, the period nonupling mode does not have the characteristics of a building block, but rather forms as a result of the coalescence of two shorter period quadrupling building blocks entering the deep post-wrinkling regime.

The inset of figure 4*a* shows that the nonupling equilibrium stems from the fifth bifurcation point BH2 on the fundamental path through an eigenmode with eight full waves. Left to right, the five bifurcation points on the fundamental path from B1 to BH2 correspond to critical eigenmodes with 9, 9.5, 8.5, 10 and eight full waves. These branching points are important because they offer the possibility for other combinations of building block localizations to form and then recombine into the final stable *n*-tupling hump. For instance, another possible loading path to a stable regular wrinkling pattern comprising building blocks is illustrated by branch-switching from point B1 (see the dashed blue line in the inset of figure 4*a*). This bifurcation leads to a stable

[1]H denotes critical points on the equilibrium path branching from higher-order bifurcation points on the fundamental path.

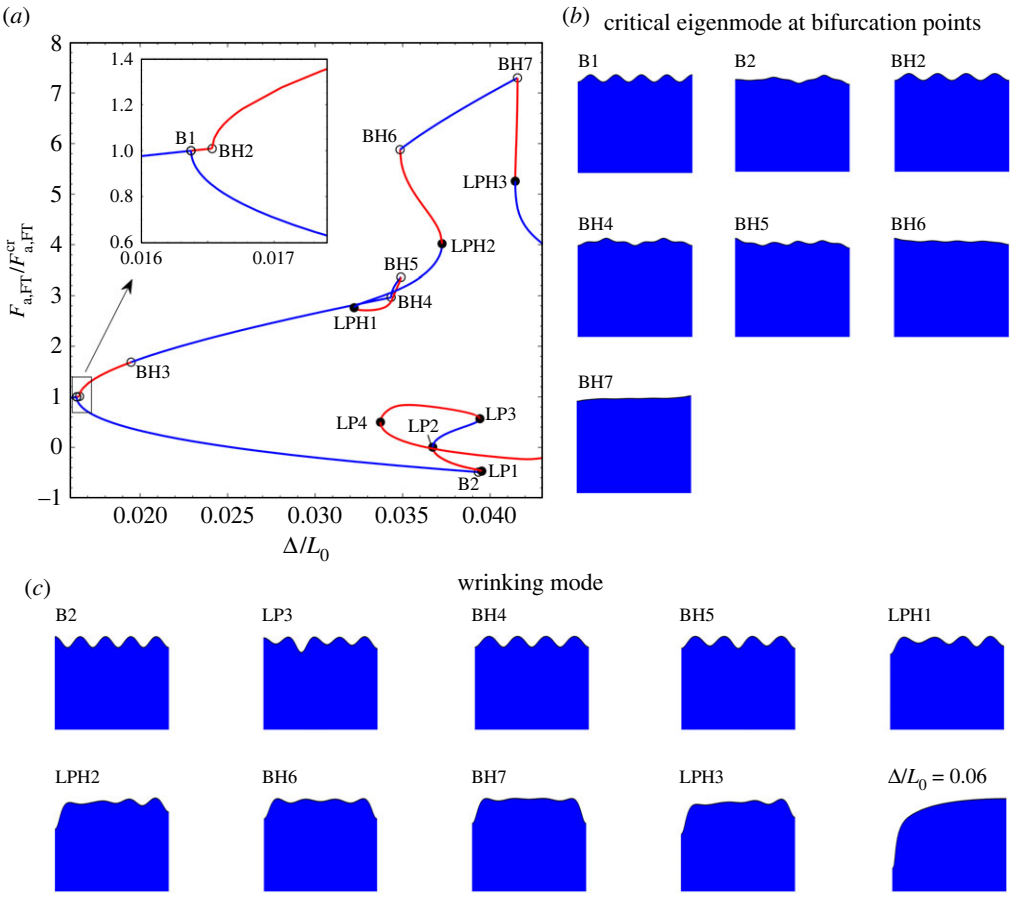

Figure 5. (*a–c*) Equilibrium path and wrinkling modes of a bilayer with length $L_0 = 4.455L_{crw}$ and pre-compression strain in the substrate of 0.7. Detailed annotations in the figure are as described in figure 3. The path leading to period quadrupling bifurcates from the second bifurcation point on the fundamental path BH2. Under natural loading (monotonically increasing end-shortening), the bilayer bifurcates at B1 and follows the primary path to B2. (Online version in colour.)

wrinkling mode with nine waves, which then evolves into stable period sextupling (one and a half humps over the length of the domain) in the intermediate strain regime (see figure 14 in the electronic supplementary material for more details). As B1 represents the lowest bifurcation point on the fundamental path, assuming a perfect system, this loading path to period sextupling would thus be the natural wrinkling evolution under monotonically increasing end-compression. In summary, the bilayer of length $L_0 = 9L_{crw}$ does not form period nonupling as a result of sequential symmetry-breaking and -restoring in the intermediate strain regime but rather forms period n-tupling modes of lower order, which then merge to form period nonupling in the deep post-wrinkling regime.

(c) $L_0 = 4.455L_{crw}$

In the preceding two subsections, we explored the bifurcation diagrams of bilayers with length equal to an integer multiple of the critical wrinkling wavelength. In practice, the length of bilayers is rarely exactly an integer multiple of L_{crw}. Moreover, the symmetry boundary conditions adopted at both ends of the bilayer also accommodate half waves along the bilayer length. Therefore, it is also important to understand the wrinkling behaviour of bilayers with lengths equal to a non-integer number of the critical wavelength.

Here, a bilayer with $L_0 = 4.455L_{crw}$ is selected and figure 5 presents its equilibrium path. The bifurcation structure is similar to the previous case of $L_0 = 9L_{crw}$ in figure 4, with the caveat that in the shorter case certain symmetry-breaking bifurcation points vanish. This is because the boundary condition at one end of the shorter bilayer is effectively located at the mid-length of the longer system, which, in contrast, is devoid of restraints. Hence, the longer system is free to break symmetry about its mid-length, while the shorter system cannot about its boundary. The first two bifurcation points on the fundamental equilibrium path of the flat bilayer feature 4.5 and 4 sinusoidal waves, see points B1 and BH2 in figure 5, respectively. Branch-switching from the first (critical) bifurcation point B1 leads to a stable periodic wrinkling mode with 4.5 waves. However, further branch switching along the ensuing sinusoidally wrinkled equilibrium path does not lead to additional stable wrinkling patterns.

Branch-switching from the second bifurcation point on the fundamental path (BH2) initially leads to an unstable equilibrium path with four sinusoidal waves, but this sinusoidal wrinkling mode stabilizes at the bifurcation point BH3. With further loading, period doubling initiates at bifurcation point BH4 and remains stable up to bifurcation point BH5. The critical eigenvector of point BH4 in figure 5*b* features the characteristic period doubling mode (two outwards humps), which is added to the sinusoidal wrinkling state of point BH4 itself (figure 5*c*). Branch-switching from the bifurcation point BH5 leads to sequential snap-back and snap-through instabilities, see LPH1 and LPH2 in figure 5*c*, with associated irregular and non-symmetric wrinkling patterns. The symmetry of the wrinkling mode is restored at bifurcation point BH6, where stable period quadrupling—a stable building block—forms. Further loading into the advanced strain regime then causes further period doubling, leading to a half hump with a fold localization at one end (see $\Delta/L_0 = 0.06$ in figure 5*c*). Thus, the pattern formation for this bilayer with overall length equal to a non-integer multiple of the critical wavelength L_{crw} follows the same sequence as all integer-length bilayers detailed in §4 of the electronic supplementary material and summarized in figure 1*b*.

4. Building block mechanics, domain of existence, energetics and spatial chaos

(a) Wrinkling pattern progression summary and further insights

From all the analyses in the range $L_0 = [4, \ldots, 9]L_{crw}$ (which are discussed in §4 of the electronic supplementary material for the sake of conciseness), a set of stable period n-tupling modes were identified that are confined by inward localizations (folds) at either end of the wrinkling pattern. These newly observed n-tupling modes (figure 1) are period quadrupling, quintupling, sextupling, septupling and octupling, and are identified as the 'building blocks' that govern the intermediate post-critical regime of long, pre-compressed bilayers beyond the initial wrinkling regime, i.e. the sinusoidal or period doubling modes at small values of end compression. In many cases, these n-tupling modes form through breaking and restoring of symmetry groups in regions of intermediate values of end-compression with multiple stable equilibria, and it is these transition modes, not 'chaos' [18], that help to explain the irregular patterns observed in experiments. With further loading beyond the intermediate post-wrinkling regime and into the deep post-wrinkling range, the individual n-tupling localizations—the building blocks—may merge with their neighbouring ones through further period doubling events, until eventually a crease forms through self-contact across imposed symmetry lines.

With no pre-compression in the substrate, the wrinkling pattern progression under end-compression is sequential period doubling and the symmetry of the system is always preserved [21,26]. Conversely, in cases with pre-strained substrates analysed here, period doubling bifurcations are confined to the initial and deep post-critical regimes. Hence, pre-compressing the substrate has an outsized effect on the intermediate post-wrinkling regime, highlighting the importance of the identified building blocks.

The mechanics of period doubling bifurcations in a compressed bilayer with no pre-compression in the substrate has previously been described using an analogous system

comprising a beam on nonlinear elastic foundations (e.g. Brau *et al.* [21]). In this system, the wrinkling pattern formation is governed by the leading-order linear stiffness term of the foundation and a sinusoidally wrinkled state represents an energetic compromise between the global Euler mode preferred by the stiff beam, and, on the other hand, the minimization of the individual springs' extensions/shortenings preferred by the foundation. As the amplitude of the wrinkles increases with growing compression of the bilayer, the first nonlinear term of the foundation stiffness starts to govern the mechanics. When the substrate is in a state of compression, this is a quadratic nonlinear term [19] that corresponds to an up-down asymmetry with preferential deformation into the substrate. This characteristic of the substrate leads to a period doubling bifurcation, whereby the uniform distribution of bending energy in the sinusoidal wrinkling state is replaced by concentrated bending energy in localized inward folds and segments of reduced curvature in between. With further compression, this phenomenon repeats at another period doubling bifurcation to form period quadrupling and further concentration of bending energy in a smaller number of folds. Our analyses show that pre-compressing the substrate intensifies the asymmetric up-down nonlinearity of the substrate leading to immediate period n-tupling bifurcations. In this regard, the behaviour of a highly strained stiff film on an elastic substrate approaches the behaviour of a stiff film on a liquid substrate, whereby, in the latter case, the film immediately transitions into a single localized inward fold [22]. While the foundation stiffness of a liquid substrate is sufficiently nonlinear to allow for localizations to bifurcate from the flat fundamental state, the foundation stiffness of an elastic substrate gradually increases its quadratic nonlinearity as either pre-compression and/or applied mechanical compression increase, thereby passing through a sequence of sharper and sharper localizations.

(b) On the domain of existence of building blocks: length limits and creases

The identified building blocks are intermediate n-tupling states between the initial short-wavelength (sinusoidal or period doubling) wrinkling modes and the overall hump mode at high strain levels. Similarities exist between the equilibrium manifolds of these basic building blocks, and hence, it is useful to gain further insight into their characteristics. Specifically, all n-tupling modes start and end at bifurcation points with anti-symmetric critical eigenmodes that break/restore the left-right symmetry of the wrinkling pattern (see B4 and B5 in figure 3 for the bilayer with $L_0 = 5L_{\mathrm{crw}}$; BH6 and BH7 in figure 5 for the bilayer with $L_0 = 4.455L_{\mathrm{crw}}$; and further cases in §4 of the electronic supplementary material). When these two bifurcation points merge and disappear in parameter space, i.e. at a codimension-2 cusp catastrophe, the stable period n-tupling mode ceases to exist. The cusp can thus be used to determine the limit bilayer length for which a stable building block exists at all.

A multi-parameter continuation of bifurcation point B4 in figure 3, that is where stable period quintupling forms for a bilayer with $L_0 = 5L_{\mathrm{crw}}$, is conducted. Figure 6*a* shows the locus of bifurcation points traced in the end-compression *versus* bilayer length parameter space. For illustration purposes, the equilibrium path of bilayers with $L_0 = 4.455L_{\mathrm{crw}}$ and $L_0 = 4.720L_{\mathrm{crw}}$ are also shown as cutsets through the multi-dimensional equilibrium surface. The cusp is found at $L_0 = 4.331L_{\mathrm{crw}}$, where bifurcation point B4 merges with another bifurcation point and annihilates. Physically, this implies that no stable building block can exist for $L_0 < 4.331L_{\mathrm{crw}}$. Thus, for the specific material properties and substrate pre-compression level assumed here, the shortest individual wrinkling pattern bounded by inward fold localizations that can form is a period quadrupling cell of length $4.331L_{\mathrm{crw}}$.

Similarly, the upper length boundary for the existence of a stable building block as an individual cell confined by inward folds is determined using the ability to trace limit points through parameter space. Specifically, limit point LPH3 of figure 5 denotes the point where a half hump mode stabilizes for a bilayer of length $L_0 = 4.555L_{\mathrm{crw}}$. Hence, this limit point is equivalent to a full hump forming for a system of twice this length ($L_0 = 9.11L_{\mathrm{crw}}$). This can be observed in figure 4, where LPH3 denotes the point where two period quadrupling building blocks merge

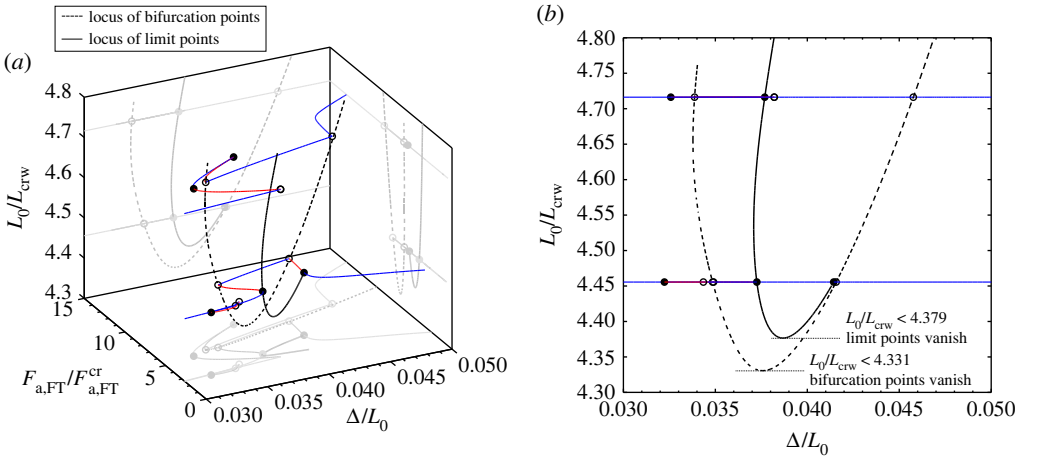

Figure 6. (*a* and *b*) Locus of the bifurcation points (dashed curves) and limit points (solid black curves) of bilayers with different lengths. Also shown are the equilibrium paths of bilayers with $L_0 = 4.455L_{crw}$ and $L_0 = 4.720L_{crw}$. Note that the bifurcation structure of the bilayer with $L_0 = 4.455L_{crw}$ is essentially the same as the bilayer with $L_0 = 8.910L_{crw}$ comprising two building blocks of length $4.455L_{crw}$. (Online version in colour.)

into a period nonupling mode that governs the deep post-wrinkling regime. As was discussed in §3b, the period nonupling mode is therefore not a building block in itself, but forms by the coalescence of two period quadrupling building blocks. As a result, if LPH3 is path-followed with decreasing L_0, then a certain bilayer length must exist, below which, two building blocks can no longer merge to form a period nonupling mode. Indeed, below this critical length we would expect a stable period octupling mode rather than two stable period quadrupling modes that coalesce into period nonupling. Thus, LPH3 is traced through the end-compression *versus* bilayer length parameter space, where for simplicity, we choose the equivalent point LPH3 of the half-length system, i.e. $L_0 = 4.455L_{crw}$. If LPH3 vanishes at a cusp by merging with another limit point, then we have identified the upper length boundary of the stable building blocks in the intermediate strain regime, as for any bilayer longer than this, the system breaks into two shorter building blocks.

As predicted, LPH3 vanishes at a cusp when $L_0 = 4.379L_{crw}$ (see figure 6*b*), where it merges with LPH2. For the equivalent full length system, this corresponds to a critical bilayer length of $L_0 = 2 \times 4.379L_{crw} = 8.758L_{crw}$. This implies that when the bilayer is shorter than $L_0 = 8.758L_{crw}$, a stable n-tupling building block exists that covers the entire length of the bilayer (inward localization at either end). However, for bilayers longer than $L_0 = 8.758L_{crw}$, the system cannot form a stable building block that extends along the entire length of the bilayer in the intermediate strain regime, and rather breaks into two shorter building blocks.

In conclusion, stable building blocks of the intermediate strain regime can exist only for bilayers extensions in the range $[4.331, 8.758]L_{crw}$. An approximate, first-order approach to determine the upper and lower length boundaries of each individual n-tupling building block is discussed in §4c. As we will see in §5, this estimation can be used to program the wrinkling pattern of longer bilayers.

Since the effects of creasing (contact across reflective symmetry lines) are not accounted for in the model, it is also important to identify the longest possible hump mode before creasing occurs. To do this, a multi-parameter continuation of the furthest bifurcation point where period doubling occurs is conducted. In this case, the bilayer with $L_0 = 8L_{crw}$ (the equilibrium path can be found in §4.1.6 of the electronic supplementary material) is selected as a starting point and the length of the bilayer is then smoothly increased to trace the selected bifurcation point in parameter space. For the bilayer with geometry and material properties presented in table 1, it is found that creasing

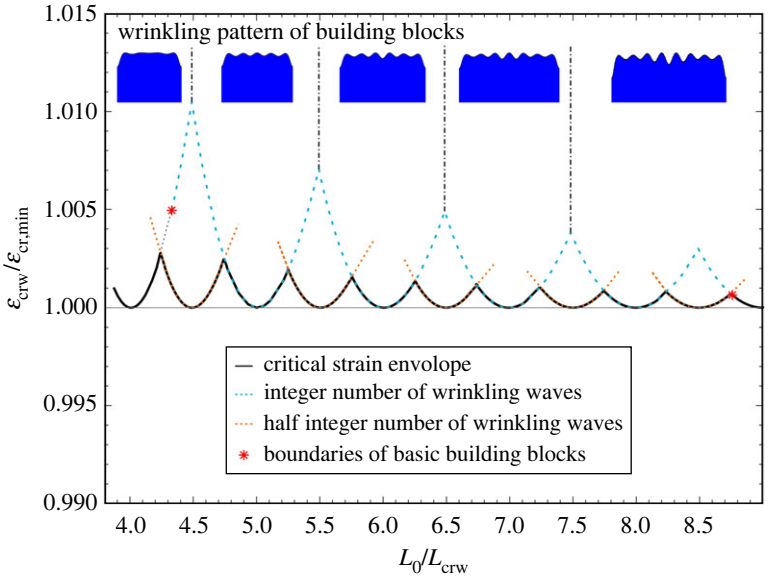

Figure 7. The relationship between the nominal critical wrinkling strain (transition from flat to sinusoidally wrinkled states) and bilayer length. The solid black curves represent the envelope of the critical strain; the dotted blue and orange curves represent the wrinkling modes with integer number and half-integer number of full waves, respectively. The number of wrinkling waves in each envelope hump is equal to the *x*-coordinate of the minimum of the hump (an integral or half-integer number). The representative *n*-tupling wrinkling modes of the corresponding building block for each hump are also shown. (The wrinkling pattern corresponds to the bifurcation point where the stable building block is formed, e.g. B4 for $L_0 = 5L_{crw}$ in figure 3). Red stars represent the lower and upper boundaries of the basic building blocks that are discussed in §4b. The geometry and material properties of the bilayer are presented in table 1; the pre-compression factor in the substrate is $\lambda_{pre} = 0.7$. L_0 and L_{crw} are the length of the film (length of the substrate after pre-compression) and the critical wrinkling wavelength of an infinitely long bilayer, respectively. ε_{crw} is the nominal critical wrinkling strain; $\varepsilon_{cr,min}$ is the minimal critical wrinkling strain, i.e. the critical strain of an infinitely long bilayer. (Online version in colour.)

occurs for $L_0 = 8.3L_{crw}$ in a half-hump mode. Below this length, further period doubling of the basic building blocks can occur without the formation of a crease. This implies that the longest full hump mode that can be formed by the coalescence of individual *n*-tupling building blocks is $L_0 = 16.6L_{crw}$.

(c) Approximate estimation of the building blocks' upper and lower lengths

For given material and geometric properties, the loci of bifurcation points traced in the previous subsection may be used to determine which building blocks can form for varying L_0, as well as their minimum/maximum extension. However, tracing these curves in parameter space can be computationally expensive. Moreover, the extensive exploration of the bifurcation landscape for bilayers with different lengths (see above and §4 of the electronic supplementary material) indicates that the initial buckling modes along the fundamental path (the flat state) can provide insight into the building blocks that will form for a bilayer of given length.

Figure 7 presents the relationship between the nominal critical wrinkling strain, ε_{crw} (transition from flat to sinusoidal wrinkles), with respect to L_0. The curves are obtained using the pitchfork continuation solver of the in-house FE code [36] (more details can be found in §3 of the electronic supplementary material). The critical strain is normalized by the corresponding value for an infinitely long bilayer, $\varepsilon_{cr,min}$, while L_0 is normalized by L_{crw}. The curves describing the first and second bifurcation points on the fundamental path—in this case wrinkles of an integer number (blue curve) of full waves and a half-integer number (orange curve) of full waves—are

intertwined, in a manner reminiscent of the critical buckling curves of axially compressed flat plates (critical buckling stress *versus* aspect ratio) [40]. The effective critical wrinkling strain is given by the lower-bound envelope of the integer and half-integer curves. Hence, for bilayers with a half-integer number of full waves in the critical (first) eigenmode, the second eigenmode always features an integer number of full waves, and *vice versa*. For instance, a bilayer of length $L_0 = 4.455L_{\mathrm{crw}}$ bifurcates onto a pattern with 4.5 waves first. By not branch switching, i.e. continuing along the now unstable fundamental path of flat solutions, the second bifurcation point corresponds to a wrinkled pattern with four waves. Similarly, a bilayer with $L_0 = 4.720L_{\mathrm{crw}}$ would still have 4.5 waves in the first critical eigenmode, but five in the second.

Noting that the upper and lower boundaries of the domain of existence for building blocks, which were determined in the preceding section, are labelled as red stars, our analyses indicate that, for bilayers of generic length, a good first-order prediction of the stable n-tupling mode that forms in the intermediate post-wrinkling range (i.e. the building block) can be obtained by splitting figure 7 into vertical sections extending between the peaks of the blue curves. As a result, the bilayers of length $L_0 = 4.455L_{\mathrm{crw}}$ and $L_0 = 4.720L_{\mathrm{crw}}$ should form period quadrupling and quintupling building blocks, respectively, and this is indeed what is observed with more detailed explorations of the post-wrinkling bifurcation landscape (see §4.2 of the electronic supplementary material).

There is, of course, a natural limit to using figure 7 as a first-order approximation for which building block forms in a bilayer's intermediate post-wrinkling regime, as well as its upper and lower extension bounds. As the bilayer lengthens, the bifurcation points on the fundamental path are more tightly spaced and the post-wrinkling bifurcation structure becomes more complex. For example, for a bilayer of length $L_0 = 8.7L_{\mathrm{crw}}$ the second bifurcation point may feature nine waves in the eigenmode, but in the intermediate strain range the bilayer splits into two blocks of length $L_0 = 4.35L_{\mathrm{crw}}$, each featuring a period quadrupling mode, or alternatively, form a single block featuring a period octupling mode.

(d) Strain energy density of basic building blocks and spatial chaos

The existence of an upper length boundary over which building blocks cannot form as single entities has immediate implications on the behaviour of long bilayers, i.e. bilayers longer than the upper threshold of $8.758L_{\mathrm{crw}}$. In these cases, the variety of stable building blocks that exist, each with different characteristic periods, can lead to the coexistence of 'competing' wrinkling patterns. This is because a bilayer longer than $L_0 > 8.758L_{\mathrm{crw}}$ naturally wrinkles into a series of adjacent n-tupling building blocks. For example, a system of length $L_0 = 20L_{\mathrm{crw}}$ can split into four period quintupling modes; or two period septupling and one period sextupling mode; or two period sextupling and one period octupling mode; and so on. The set of competing solutions is the group of all permutations of building blocks that can tessellate the bilayer's extension. The formation of a specific wrinkling pattern of adjacent building blocks depends on the strain energy of each solution as well as the starting conditions, i.e. initial imperfections and material heterogeneity of the bilayer. To the limit of a perfect and infinitely long bilayer, the system's response becomes spatially chaotic [37]. Conversely, with the acquired understanding of the basic building blocks, we can tailor and pre-program the formation of periodic wrinkling patterns in long bilayers. One of the potential approaches along these lines is discussed in §5.

Auguste *et al.* [18] compared the strain energy of different stable period n-tupling modes and proposed that the wrinkling mode with lowest strain energy is, all else being equal, most likely to occur due to its state as a global energy minimizer. Following a similar train of thought, it is beneficial to calculate the strain energy density of each stable building block in order to ascertain its likelihood of forming in long bilayers. Figure 8 presents the strain energy density of each building block (strain energy per unit length) at different nominal strain levels, starting from the bifurcation point where each building block becomes stable and ending at the first successive instance of period doubling. Note that for the period quadrupling mode, bilayer with $L_0/L_{\mathrm{crw}} = 4.455$ was selected, since the lower boundary of building block is $4.331L_{\mathrm{crw}}$. For other

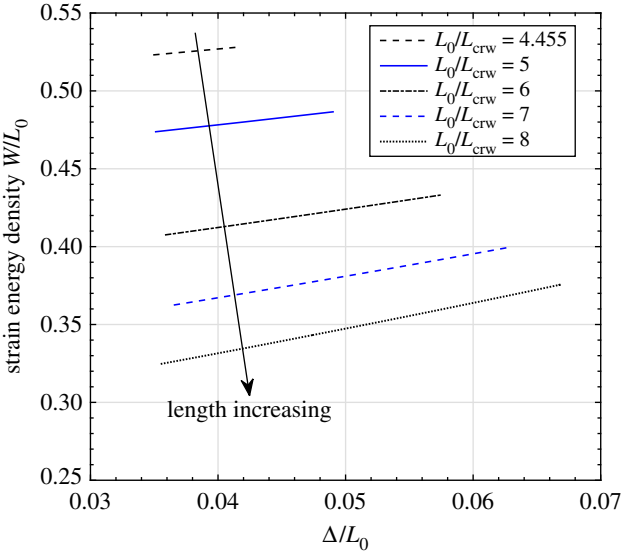

Figure 8. The strain energy density of different basic building blocks, i.e. n-tupling modes with $n = \{4, \ldots, 8\}$, in the intermediate post-wrinkling regime. The lines start and end at the bifurcation points where stable period n-tupling modes form and further period doubling occurs, respectively. (Online version in colour.)

n-tupling modes, the length of bilayers is equal to an integer multiple of the critical wrinkling wavelength. Generally speaking, the strain energy density decreases as the length of the building block increases. This is reasonable since longer building blocks have less curvature in the film and also form shallower localizations at their ends.

However, even though the bilayer favours the formation of wrinkling patterns with longer wavelengths, different n-tupling wrinkling patterns may be separated by unstable equilibria and hence energy barriers may prevent spontaneous transitioning of the system from a local energy minimum to the global energy minimizer. For very long bilayers—strictly much longer than the upper length boundary of the basic building blocks, $L_0 \gg 8.758L_{crw}$—a number of different stable n-tupling modes can therefore form side-by-side along the length of the bilayer, each trapped in a local energy minimum. As a result, an infinitely long bilayer will form one possible wrinkling pattern out of a strictly infinite set of possible combinations of building blocks (for instance, see figure 1*d*). In the geometrically perfect case, such a spatially chaotic system [37] is characterized by an infinite number of possible post-critical equilibrium paths. In the inherently imperfect world of manufactured bilayers, on the other hand, the morphological evolution can be controlled by defining the nature of the starting conditions rather than leaving them to chance. This idea of programming the morphological evolution of spatially chaotic bilayers using manufactured defects is what we explore next.

5. Tailoring the wrinkling pattern of long bilayers

High-fidelity manufacturing methodologies are required for the production of instability-induced morphologies for use in thin-film technologies [6–9]. However, exerting sufficient processing control over pre-compressed thin-film bilayers that may assume multiple stable shapes upon end shortening, or even exhibit spatially chaotic behaviour, can be difficult and expensive. Nonetheless, in addition to having enabled the acquisition of new understanding over their behaviour, the ability to trace a bilayer's full equilibrium manifold opens another opportunity: *modal nudging* [41,42]. Modal nudging is a recently developed design philosophy that uses the deformation modes associated with stable post-critical equilibria to alter the undeformed baseline geometry of a structure, thereby favouring the seeded postbuckling response over potential

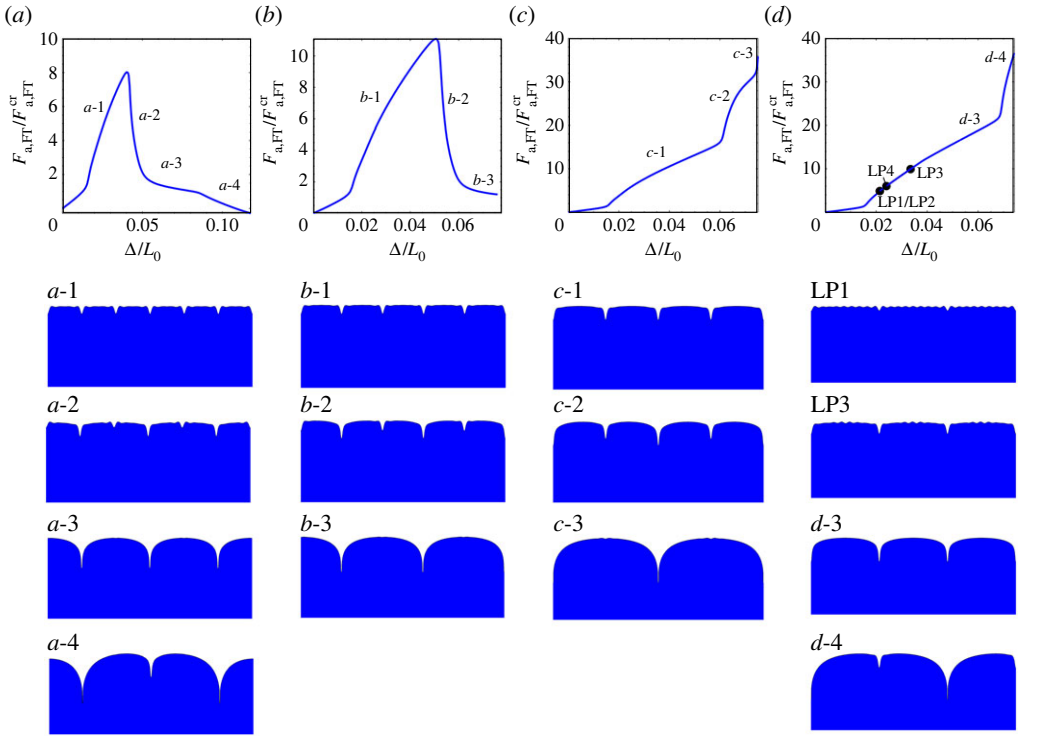

Figure 9. Equilibrium path and wrinkling modes of a bilayer of length $L_0 = 26L_{crw}$ with localized dents in the stiff film that divide the bilayer into (*a*) six, (*b*) five, (*c*) four and (*d*) three equal-length segments. Note that the locations of the localized imperfections are embedded at the valleys of stable building blocks. Random imperfections are also introduced throughout the entire length of the film. (Online version in colour.)

alternatives. Our aim here is to precondition the wrinkling response of long bilayers away from spatial chaos by embedding characteristic geometric patterns into the stiff film/substrate assembly such that the system's behaviour overall is nudged into the desired wrinkling pattern.

Figure 9 presents the equilibrium paths and wrinkling mode progression of a long bilayer with $L_0 = 26L_{crw}$ and manufactured localized dents. The distance between consecutive dents is equal to the period of stable building blocks as determined in previous sections. Different permutations of dent spacing divide the bilayer into 3–6 segments of equal length, corresponding to panels (*d*) to (*a*) in the figure. Spatially uncorrelated random imperfections are also seeded into the FE mesh of the film to test the robustness of the nudged response. The profile of the localized dents is cosinusoidal, while the amplitudes of the artificial dents and random imperfections are $0.1h_f$ and $0.005h_f$, respectively.

Our numerical results show that, with the embedded dents, the bilayers can be pre-programmed to wrinkle directly into a target pattern comprising a sequence of stable building blocks. The pattern is attained without the unstable symmetry breaking/restoring that would be observed in the geometrically perfect case. As the equilibrium paths of all nudged cases are generally stable throughout, or feature limited regions of instability like in figure 9*d*, the behaviour of the tailored bilayers is no longer chaotic or sensitive to imperfections or uncertainties. Specifically, humps are formed between embedded localized dents.

In summary, experimentally, individual building blocks in a long, unnudged bilayer [18] are free to compete and the final wrinkling pattern is an unspecified series of adjacent building blocks dictated by the profile of imperfections present in the bilayer. Conversely, in bilayers pre-programmed by modal nudging, the morphological evolution can be designed and controlled. In either case, with further end-compression beyond the intermediate strain range, the initially developed building blocks undergo further period doubling by merging with their neighbouring

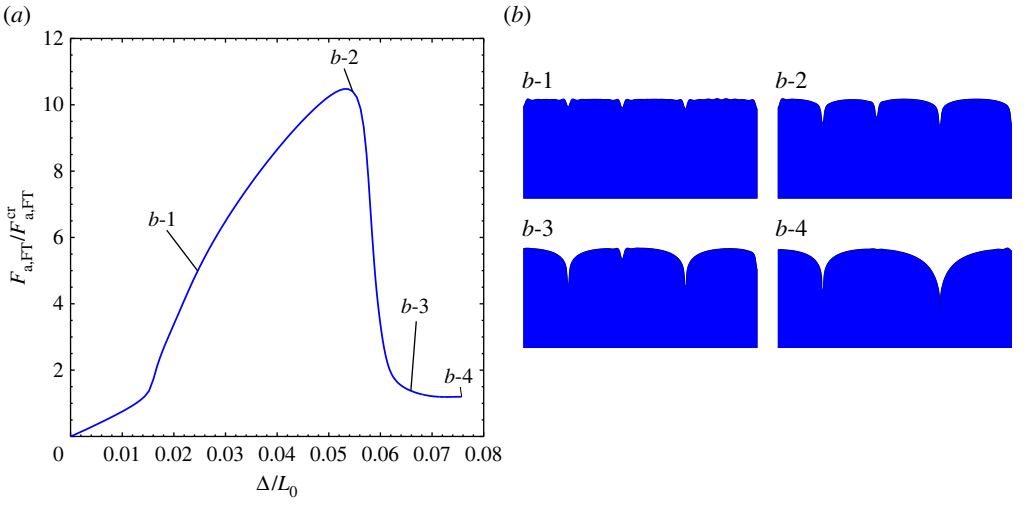

Figure 10. (*a* and *b*) Equilibrium path and wrinkling modes of a bilayer with length $L_0 = 26L_{crw}$ and artificially localized dents in the stiff film that divide the bilayer into four segments of length $5L_{crw}$, $6L_{crw}$, $7L_{crw}$ and $8L_{crw}$. The details are the same as in figure 9. (Online version in colour.)

building blocks to form longer humps until self-contact occurs. However, this evolution is engineered in the nudged case and completely controlled by random imperfections in the unnudged case.

Of particular note in figure 9 is the bilayer divided into three segments of panel (*d*), because, unlike the other cases, the bifurcation diagram features some limit points (two pairs) along the equilibrium path, before three humps are formed. These limit points correspond to snap-back and snap-through instabilities where the wrinkling patterns within the left and right building blocks change, with the number of sinusoidal waves therein going from nine to eight. This is not observed in the other three cases with more dents and with building blocks of shorter length. This phenomenon occurs because, with an increase in cell length, the bifurcation diagram of the corresponding building block becomes increasingly more complex. Longer building blocks cannot be obtained directly through monotonic increases in end-compression (see §§4.1.5 and 4.1.6 of the electronic supplementary material for bilayers with $L_0 = 7L_{crw}$ and $L_0 = 8L_{crw}$). In these cases, instabilities are present along the path to pattern formation. Hence, background imperfections play a relatively bigger role in comparison with shorter building blocks. As a consequence, the size of the dents introduced to produce the results in figure 9 becomes increasingly less efficient at exerting sufficient control over the response. In other words, with longer building blocks, we lose some 'nudging authority' [43] over the precise wrinkling sequence that is to be imposed. Additional geometric nudging, e.g. deeper dents or more defined profiles, is thus required to guarantee effective control over the wrinkling progression and the final pattern. For instance, additional shallower dents can be introduced between the original larger dents.

As a final example of nudging, figure 10 presents a combination of different basic building blocks, i.e. the distance between dents corresponds to $5L_{crw}$, $6L_{crw}$, $7L_{crw}$ and $8L_{crw}$. Stable wrinkling patterns corresponding to these four basic building blocks are observed in the intermediate strain level. With further compression, the building blocks merge with their neighbouring building blocks to form humps with longer characteristic lengths. As above, the wrinkling progression has been successfully pre-programmed.

6. Conclusion

We have used the versatility of a generalized path-following FE framework to uncover the bifurcation landscape of end-compressed bilayers that comprise a stiff film mounted on a

pre-compressed soft substrate. Compared with cases where the substrate is unstrained, the pre-compressed bilayer features subcritical bifurcations, multi-stability and imperfection sensitivity that provide challenges in modelling and experimentation. Crucially, our models allow a comprehensive exploration of the bifurcation behaviour of bilayers of different lengths and thereby help to uncover different phenomena that govern the bilayer's mechanics. For all bilayer lengths considered, the initially flat, stiff film wrinkles into a periodic sinusoidal pattern and then undergoes further bifurcations that increase the wavelength of the wrinkling pattern as the applied compression increases. For bilayers with an unstrained substrate, period doubling and period tripling bifurcations are well documented. For the case of a pre-compressed substrate studied here, period quadrupling, quintupling, sextupling, septupling and octupling modes are also possible depending on the length of the bilayer. These period n-tupling modes are here identified as stable 'building blocks' that govern the intermediate post-wrinkling regime. They form as a result of sequential subcritical pitchfork and saddle node bifurcations that first break and then restore symmetry groups. As compression is increased even further beyond this intermediate post-wrinkling regime, the building blocks coalesce via supercritical bifurcations until creases (self-contact) occur. In this manner, the behaviour of the pre-compressed bilayer returns to the behaviour of the initially unstrained bilayer governed by sequential period doubling bifurcations, once sufficient end-compression is applied.

In addition, we have identified multiple, coexisting but isolated stable states that lead to occasionally irregular wrinkling patterns in the load region over which the transition from sinusoidal wrinkling to period n-tupling occurs. Furthermore, for some levels of compression, the irregular patterns coexist with periodic solutions, thereby explaining the seemingly 'chaotic' and uncontrollable, but actually just irregular and multivalued, pattern formation observed in previous experiments.

As bilayer length increases, the different n-tupling modes compete during the pattern formation sequence. Indeed, different permutations of the n-tupling building blocks can tesselate the bilayer's length, and the exact permutation formed is a function of the initial condition. In this manner, the pre-compressed bilayer features the properties of pronounced imperfection sensitivity, and in the limit of an infinitely long bilayer is governed by spatial chaos with infinite possible permutations of the building blocks. As a corollary, this means that the permutation of building blocks that form in long bilayers can be tailored by precisely controlling the initial conditions. Aiming to aid manufacturing of bilayers for thin-film technologies, we demonstrate that the post-wrinkling pattern can be programmed in a deterministic way using the concept of 'modal nudging' [41]. This programming is achieved by embedding multiple localized dents in the stiff film, spaced at intervals equal to the length of the identified building blocks. Future work will focus on manufacturing and testing nudged bilayers to validate the ability to program the wrinkling patterns experimentally.

Data accessibility. The dataset supporting this article has been uploaded as part of the electronic supplementary material [44].

Authors' contributions. J.S.: conceptualization, data curation, formal analysis, investigation, methodology, software, validation, visualization, writing—original draft; A.P.: conceptualization, funding acquisition, project administration, resources, supervision, writing—review and editing; R.M.J.G.: conceptualization, funding acquisition, methodology, project administration, resources, software, supervision, writing—review and editing.

All authors gave final approval for publication and agreed to be held accountable for the work performed therein.

Conflict of interest declaration. We declare we have no competing interest.

Funding. This work was funded by the Leverhulme Trust through a Philip Leverhulme Prize awarded to R.M.J.G. R.M.J.G. is also funded by the Royal Academy of Engineering under the Research Fellowship scheme (RF/201718/17178). A.P. was funded by the Engineering and Physical Sciences Research Council (EPSRC) under their Research Fellowship scheme (EP/M013170/1). The support of all funders is gratefully acknowledged.

References

1. Li B, Cao YP, Feng XQ, Gao H. 2012 Mechanics of morphological instabilities and surface wrinkling in soft materials: a review. *Soft Matter* **8**, 5728–5745. (doi:10.1039/c2sm00011c)
2. Eskandari M, Pfaller MR, Kuhl E. 2013 On the role of mechanics in chronic lung disease. *Materials* **6**, 5639–5658. (doi:10.3390/ma6125639)
3. Ciarletta P, Balbi V, Kuhl E. 2014 Pattern selection in growing tubular tissues. *Materials* **113**, 248101. (doi:10.1103/physrevlett.113.248101)
4. Kuhl E. 2016 Biophysics: unfolding the brain. *Nat. Phys.* **12**, 533–534. (doi:10.1038/nphys3641)
5. Tallinen T, Chung JY, Rousseau F, Girard N, Lefèvre J, Mahadevan L. 2016 On the growth and form of cortical convolutions. *Nat. Phys.* **12**, 588–593. (doi:10.1038/nphys3632)
6. Kim JB, Kim P, Pégard NC, Oh SJ, Kagan CR, Fleischer JW, Stone HA, Loo YL. 2012 Wrinkles and deep folds as photonic structures in photovoltaics. *Nat. Photonics* **6**, 327. (doi:10.1038/nphoton.2012.70)
7. Yu C, Masarapu C, Rong J, Wei B, Jiang H. 2009 Stretchable supercapacitors based on buckled single-walled carbon-nanotube macrofilms. *Adv. Mater.* **21**, 4793–4797. (doi:10.1002/adma.200901775)
8. Stafford CM, Harrison C, Beers KL, Karim A, Amis EJ, VanLandingham MR, Kim HC, Volksen W, Miller RD, Simonyi EE. 2004 A buckling-based metrology for measuring the elastic moduli of polymeric thin films. *Nat. Mater.* **3**, 545–550. (doi:10.1038/nmat1175)
9. Yang S, Khare K, Lin PC. 2010 Harnessing surface wrinkle patterns in soft matter. *Adv. Funct. Mater.* **20**, 2550–2564. (doi:10.1002/adfm.201000034)
10. Wang Q, Zhao X. 2014 Phase diagrams of instabilities in compressed film-substrate systems. *J. Appl. Mech.* **81**, 051004. (doi:10.1115/1.4025828)
11. Shield TW, Kim KS, Shield RT. 1994 The buckling of an elastic layer bonded to an elastic substrate in plane strain. *J. Appl. Mech.* **61**, 231–235. (doi:10.1115/1.2901434)
12. Li B, Zhao HP, Feng XQ. 2011 Spontaneous instability of soft thin films on curved substrates due to van der Waals interaction. *J. Mech. Phys. Solids* **59**, 610–624. (doi:10.1016/j.jmps.2010.12.009)
13. Jin L, Takei A, Hutchinson JW. 2015 Mechanics of wrinkle/ridge transitions in thin film/substrate systems. *J. Mech. Phys. Solids* **81**, 22–40. (doi:10.1016/j.jmps.2015.04.016)
14. Holland M, Li B, Feng X, Kuhl E. 2017 Instabilities of soft films on compliant substrates. *J. Mech. Phys. Solids* **98**, 350–365. (doi:10.1016/j.jmps.2016.09.012)
15. Cao Y, Hutchinson JW. 2012 Wrinkling phenomena in Neo-Hookean film/substrate bilayers. *J. Appl. Mech.* **79**, 031019. (doi:10.1115/1.4005960)
16. Sun JY, Xia S, Moon MW, Oh KH, Kim KS. 2012 Folding wrinkles of a thin stiff layer on a soft substrate. *Proc. R. Soc. A* **468**, 932–953. (doi:10.1098/rspa.2011.0567)
17. Liu J, Bertoldi K. 2015 Bloch wave approach for the analysis of sequential bifurcations in bilayer structures. *Proc. R. Soc. A* **471**, 20150493. (doi:10.1098/rspa.2015.0493)
18. Auguste A, Jin L, Suo Z, Hayward RC. 2014 The role of substrate pre-stretch in post-wrinkling bifurcations. *Soft Matter* **10**, 6520–6529. (doi:10.1039/C4SM01038H)
19. Hutchinson JW. 2013 The role of nonlinear substrate elasticity in the wrinkling of thin films. *Phil. Trans. R. Soc. A* **371**, 20120422. (doi:10.1098/rsta.2012.0422)
20. Efimenko K, Rackaitis M, Manias E, Vaziri A, Mahadevan L, Genzer J. 2005 Nested self-similar wrinkling patterns in skins. *Nat. Mater.* **4**, 293–297. (doi:10.1038/nmat1342)
21. Brau F, Vandeparre H, Sabbah A, Poulard C, Boudaoud A, Damman P. 2011 Multiple-length-scale elastic instability mimics parametric resonance of nonlinear oscillators. *Nat. Phys.* **7**, 56–60. (doi:10.1038/nphys1806)
22. Brau F, Damman P, Diamant H, Witten TA. 2013 Wrinkle to fold transition: influence of the substrate response. *Soft Matter* **9**, 8177–8186. (doi:10.1039/c3sm50655j)
23. Zhao R, Zhang T, Diab M, Gao H, Kim KS. 2015 The primary bilayer ruga-phase diagram I: localizations in ruga evolution. *Extreme Mech. Lett.* **4**, 76–82. (doi:10.1016/j.eml.2015.04.006)
24. Wang Q, Zhao X. 2016 Beyond wrinkles: multimodal surface instabilities for multifunctional patterning. *MRS Bull.* **41**, 115–122. (doi:10.1557/mrs.2015.338)
25. Zhuo L, Zhang Y. 2015 The mode-coupling of a stiff film/compliant substrate system in the post-buckling range. *Int. J. Solids Struct.* **53**, 28–37. (doi:10.1016/j.ijsolstr.2014.10.028)
26. Jung JH, Bae J, Moon MW, Kim KS, Ihm J. 2015 Numerical study on sequential period-doubling bifurcations of graphene wrinkles on a soft substrate. *Solid State Commun.* **222**, 14–17. (doi:10.1016/j.ssc.2015.08.020)

27. Zhao Y, Cao Y, Hong W, Wadee MK, Feng XQ. 2015 Towards a quantitative understanding of period-doubling wrinkling patterns occurring in film/substrate bilayer systems. *Proc. R. Soc. A* **471**, 20140695. (doi:10.1098/rspa.2014.0695)
28. Li M, Sun B. 2022 Post-buckling behaviors of thin-film soft-substrate bilayers with finite-thickness substrate. *Sci. Rep.* **12**, 1–13. (doi:10.1038/s41598-022-08136-w)
29. Zang J, Zhao X, Cao Y, Hutchinson JW. 2012 Localized ridge wrinkling of stiff films on compliant substrates. *J. Mech. Phys. Solids* **60**, 1265–1279. (doi:10.1016/j.jmps.2012.03.009)
30. Chen YC, Crosby AJ. 2014 High aspect ratio wrinkles via substrate prestretch. *Adv. Mater.* **26**, 5626–5631. (doi:10.1002/adma.201401444)
31. Budday S, Andres S, Walter B, Steinmann P, Kuhl E. 2017 Wrinkling instabilities in soft bilayered systems. *Phil. Trans. R. Soc. A* **375**, 20160163. (doi:10.1098/rsta.2016.0163)
32. Saha SK. 2017 Sensitivity of the mode locking phenomenon to geometric imperfections during wrinkling of supported thin films. *Int. J. Solids Struct.* **109**, 166–179. (doi:10.1016/j.ijsolstr.2017.01.018)
33. Cheng Z, Xu F. 2021 Intricate evolutions of multiple-period post-buckling patterns in bilayers. *Sci. China: Phys., Mech. Astron.* **64**, 1–10. (doi:10.1007/s11433-020-1620-0)
34. Fu C, Cheng Z, Wang T, Xu F. 2022 An asymptotic modeling and resolution framework for morphology evolutions of multiple-period post-buckling modes in bilayers. *Math. Mech. Solids* **27**,1397–1411. (doi:10.1177/10812865221083046)
35. Eriksson A. 1998 Structural instability analyses based on generalised path-following. *Comput. Methods Appl. Mech. Eng.* **156**, 45–74. (doi:10.1016/S0045-7825(97)00200-4)
36. Groh R, Avitabile D, Pirrera A. 2018 Generalised path-following for well-behaved nonlinear structures. *Comput. Methods Appl. Mech. Eng.* **331**, 394–426. (doi:10.1016/j.cma.2017.12.001)
37. Thompson J, Virgin L. 1988 Spatial chaos and localization phenomena in nonlinear elasticity. *Phys. Lett. A* **126**, 491–496. (doi:10.1016/0375-9601(88)90045-X)
38. Bonet J, Gil AJ, Wood RD. 2016 *Nonlinear solid mechanics for finite element analysis: statics*. Cambridge, UK: Cambridge University Press.
39. Vandeparre H, Piñeirua M, Brau F, Roman B, Bico J, Gay C, Bao W, Lau CN, Reis PM, Damman P. 2011 Wrinkling hierarchy in constrained thin sheets from suspended graphene to curtains. *Phys. Rev. Lett.* **106**, 224301. (doi:10.1103/PhysRevLett.106.224301)
40. Timoshenko SP, Woinowsky-Krieger S. 1959 *Theory of plates and shells*. New York, NY: McGraw-Hill.
41. Cox B, Groh R, Avitabile D, Pirrera A. 2018 Modal nudging in nonlinear elasticity: tailoring the elastic post-buckling behaviour of engineering structures. *J. Mech. Phys. Solids* **116**, 135–149. (doi:10.1016/j.jmps.2018.03.025)
42. Cox B, Groh R, Pirrera A. 2019 Nudging axially compressed cylindrical panels toward imperfection insensitivity. *J. Appl. Mech.* **86**, 071010. (doi:10.1115/1.4043284)
43. Shen J, Groh R, Schenk M, Pirrera A. 2021 Experimental path-following of equilibria using Newton's method. Part I: theory, modelling, experiments. *Int. J. Solids Struct.* **210**, 203–223. (doi:10.1016/j.ijsolstr.2020.11.037)
44. Shen J, Pirrera A, Groh RMJ. 2022 Building blocks that govern spontaneous and programmed pattern formation in pre-compressed bilayers. Figshare. (doi:10.6084/m9.figshare.c.6179425)